

A 5D, polarised, Bethe-Heitler event generator for $\gamma \rightarrow e^+e^-$ conversion

D. Bernard^{a,*}

^aLLR, Ecole Polytechnique, CNRS/IN2P3, 91128 Palaiseau, France

Abstract

We describe a new version of the 5D, exact, polarised, Bethe-Heitler event generator of γ -ray conversions to e^+e^- , developed in the context of the HARPO project, that is able to simulate successive events with different photon energies and on different atomic targets without any substantial CPU overhead. The strong correlation between kinematic variables in the divergence of the five-dimensional differential cross section are mitigated by performing each step of the conversion in the appropriate Lorentz frame. We extend the verification range down to 1 keV above threshold and up to 1 EeV. This work could pave the way to the precise simulation of the high-performance γ -ray telescopes and polarimeters of the post-*Fermi*-LAT area.

Key words: gamma rays, pair conversion, event generator, polarised, Bethe-Heitler, Geant4

1. Introduction

The Geant4 toolkit is used for the detailed simulation of many scientific experiments that involve the interaction of elementary particles with a detector [1, 2]. For experiments with a simple geometry and that involve only electrons, positrons and photons, the EGS5 framework is also used [3, 4]. Radiation transport can also be simulated with the EGSnrc [5], Penelope [6], MCNP [7] and FLUKA [8] softwares.

The physics models of Geant4 and of EGS5 that describe the conversion of a high-energy photon to an electron-positron pair, $\gamma \rightarrow e^+e^-$, have been proven to be appropriate for the simulation of electromagnetic (EM) showers [9, 10]. These models are based on a number of approximations that limit their domains of validity [11]:

- They sample a product of independent one-dimensional (1D) probability density functions (pdf), not the five-dimensional (5D) pdf.
- They do not explicitly generate the target recoil momentum. The leptons, that is, the electron and the positron, are therefore generated incorrectly in the conversion plane.
- The polar angles of the electron and of the positron are generated independantly, so energy-momentum is not conserved. This momentum imbalance artificially creates a transverse momentum that the user could wrongly consider to be the recoil momentum, but the momentum distribution so obtained is obviously completely different from that predicted by QED.
- In most models, high-energy and/or low-polar-angle approximations are used.

Most pair telescopes, i.e., those detectors that detect the conversion of high-energy photons to a pair, consist of an active target, i.e., a detector in which the photon converts and the trajectories of the electron and of the positron (“tracks”) are measured, eventually followed by a calorimeter, in which the energy of the two leptons is measured. The photon angular resolution of pair telescopes is the combination of several contributions, that include

- the single-track angular resolution induced by the multiple scattering undergone by the lepton in the detector;
- the incorrect calculation of the momentum of the incident photon as the sum of the momenta of the final state particles, because the energy of the recoiling nucleus is too small to produce a measurable track in the detector, and the contribution of its momentum to the sum is then missing.

The existing Geant4 and EGS5 physics models are appropriate for the description of the conversion of photons in the past and present γ -ray telescopes, for which the multiple-scattering contribution dominates: the inaccurate simulation of the kinematics of the conversion and the differences between physics models are washed out by multiple scattering (Fig. 8 bottom of [11]).

Since the multiple scattering RMS of the angle of a charged particle traversing a slab of matter varies as the inverse of the track momentum, the photon angular resolution of pair telescopes degrades badly at low photon energy, that is, at low track momentum [12]. When an optimal Kalman-filter-based tracking is applied to the tracks, the multiple scattering contribution to the photon angular resolution is found to vary as $E^{-3/4}$ [13]. A coarser angular resolution affects the effectiveness of background rejection in the selection of the photons associated with a given source, and therefore degrades the point-like source sensitivity of the instrument.

*Tel 33 1 6933 5534

Email addresses: denis.bernard at in2p3.fr (D. Bernard)

A number of techniques are being developed to improve on the angular resolution with respect to that of the *Fermi*-LAT [12]. A factor of three at 100 MeV can be obtained by using all-silicon active targets, that is, without high- Z converters [14, 15] or with emulsions [16, 17]. With even lower-density homogeneous detectors such as gas time-projection chambers (TPC) a factor of ten improvement can be achieved [13] and the single-track angular resolution is so good that polarimetry has been predicted to be possible despite the dilution of the polarisation asymmetry induced by multiple scattering [18], and has actually been demonstrated by the characterisation of a TPC prototype in a particle beam [19].

For such high-performance telescopes, the single-track angular resolution is so good that the inaccuracy of the event generator becomes the main bias in the understanding of the photon angular resolution (Fig. 8 up-right of [11]). Furthermore, attempts to verify the generation of the conversion of linearly polarised photons by the physics model of Geant4 have shown a strong departure with respect to the QED prediction (Fig. 11 of [11]).

In the context of the HARPO project, we have written an exact, 5D, polarised Bethe-Heitler event generator [18]. The main difficulty in sampling the 5D differential cross section is that it diverges at small q^2 (where q is the momentum “transferred” to the target) and, for high energy, at small lepton polar angles. We first [18] solved this issue by using the BASES/SPRING [20] implementation of the VEGAS method [21]. This software proved to be excellent for the performance studies of the HARPO project, for which samples of many events were generated and then studied for given photon energy and target nucleus. But the VEGAS method first optimizes a segmentation of each of the five variable ranges corresponding to the 5D phase-space that defines the final state, after which the differential cross section is tabulated on the 5D grid obtained. These calculations prior to the generation of the first event need several seconds of CPU time which is obviously not acceptable for a particle physics simulation package like Geant4 for which the user needs to generate sequentially events with various photon energies and on various targets. The photon can either interact

- with a nucleus (nuclear conversion)

$$\gamma Z \rightarrow e^+ e^- Z;$$

- or with an electron (triplet conversion)

$$\gamma e^- \rightarrow e^+ e^- e^-.$$

This paper describes a new event generator that does not use the VEGAS method. However, it uses the same specification list as that described in [18] for the VEGAS-based generator (5D sampling, polarised, nuclear or triplet, no approximation, energy momentum conservation). After some general considerations on γ -ray conversions to pairs and their event generation (Sect. 2), we describe the part of the structure that is common to the two codes (Sect. 3). In section 4, we present some properties of the VEGAS-based generator, and in section 5, those of the new version.

Table 1: Bethe-Heitler variable list, all in the laboratory frame.

1	θ_+	positron polar angle
2	θ_-	electron polar angle
3	ϕ_+	positron azimuthal angle
4	ϕ_-	electron azimuthal angle
5	x_+	fraction of the photon energy carried by the positron

2. Bethe-Heitler, 5D, polarised, event generation

The non-polarised differential cross section was obtained by Bethe & Heitler [22], after which the calculation of the polarised cross section opened the way to polarimetry with pair conversions [23, 24, 25]. The final state can be defined by the polar angles θ_+ and θ_- , and the azimuthal angles ϕ_+ and ϕ_- , of the electron (-) and of the positron (+), respectively, and the fraction x_+ of the energy of the incident photon carried away by the positron, $x_+ \equiv E_+/E$ (Table 1. A schema can be found in Fig. 3 in [18]). All these expressions are referred to as “Bethe-Heitler” in this paper.

The two dominant Feynman diagrams were taken into account in [22], which is an excellent approximation for nuclear conversion and for high-energy triplet conversion¹: for photon energies smaller than $10 mc^2$, where m is the electron mass, neglecting the $\gamma - e$ exchange diagrams induces a relative change in the triplet total cross section smaller than 7% [26]. Only the linear polarisation of the incoming photon takes part in these expressions. The circular polarisation of the incoming photon does not take part at this first order of the Born approximation and therefore no polarisation is transferred to the leptons.

In the case where the conversion takes place in the field of an isolated, “raw”, nucleus or electron, the bare Bethe-Heitler expression mentioned above is used. In the case where the nucleus or the electron are part of an atom, the screening of the target field by the other electrons of the atom is described by a simple form factor, function of q^2 [27] (nuclear) or [28] (triplet).

This work was performed under a series of approximations:

- The nuclear form factor that affects the probability of very large- q^2 events is not considered.
- Landau-Pomeranchuk-Migdal (LPM) [29, 30] suppression effects in the differential cross-section at very high-energy are not considered.
- Any pre-existing non-zero momentum of the target prior to the conversion, such as in the case of Compton “Doppler” broadening, is not considered either.
- Coulomb corrections, due to the electromagnetic interaction between the final-state charged particles, that is prevalent, in particular, close to threshold, is not addressed.

For triplet conversion, the experimental issue of deciding which of the two negative electrons in the final state belongs

¹These two dominant diagrams are often named the Borsellino diagrams, see the discussion of Fig. 1 in [26].

Table 2: Kinematic variables and the Lorentz frame in which they are defined.

1	θ	target and pair polar angle	CMS
2	μ	e^+e^- invariant mass	
3	θ_ℓ	e^+ and e^- polar angle	pair frame
4	ϕ_ℓ	e^+ and e^- azimuthal angle	pair frame
5	ϕ	target and pair azimuthal angle	CMS

to the pair and which one is ‘‘recoiling’’ is irrelevant here: by construction, the variables ϕ_- and θ_- that take part in the Bethe-Heitler expressions refer to the electron of the pair, while q^2 refers to the recoil.

3. The two event generators: common properties

The second difficulty originates from the fact that the kinematic variables from which the differential cross section is computed cannot be computed from q^2 , the value of which drives the main divergence: the kinematic variables must be generated at random first, and then q^2 be computed from them, so some of the five variables turn out to be strongly correlated with each other. This is a general issue, even when the VEGAS method is used, as it is based on the assumption that the pdf is not too different from a product of 1D pdfs, so that a simple product of 1D segmentations of the phase space can be used.

The situation improves when computations are performed in the appropriate Lorentz systems as follows:

- The center-of-mass system (CMS) boost is determined from the values of the photon energy, E , and of the target mass, M .
- The five kinematic variables are taken at random, namely θ , μ , θ_ℓ , ϕ_ℓ and ϕ , as defined in Table 2.
- In the CMS, the target (with mass M) and the pair (with mass μ) have opposite momenta. Their 4-vectors are computed.
- The ‘‘decay’’ of the pair to an electron and a positron is performed in the pair center-of-mass frame. Their 4-vectors are computed from the pair invariant mass, μ , and from the ‘‘decay’’ polar and azimuthal angles, θ_ℓ and ϕ_ℓ . ℓ stands for lepton.
- The lepton 4-vectors are boosted ‘‘back’’ to the CMS.
- The three final particle 4-vectors (electron, positron, target) are boosted ‘‘back’’ to the laboratory frame.
- The Bethe-Heitler variables, including the polar and azimuthal angles of each particle, are obtained from the 4-vectors.
- Then the pdf for that event candidate is computed.

As the z axis is defined by the direction of the incident photon, the target recoil momentum and the pair momentum are

defining a plane that contains the photon momentum: their azimuthal angle are left unchanged upon the boost and are equal to $\pm\phi$.

Given the chosen set of kinematic variables, the final-state phase space is normalised as described in eq. (47.20) of Sect. 47.4.3 of [31]), and the differential cross section becomes

$$d\sigma = \frac{1}{(2\pi)^5} \frac{1}{32 M \sqrt{s} E} |\mathcal{M}|^2 |p_+^*| |p_r| d\mu d\Omega_+^* d\Omega_r, \quad (1)$$

where (p_+^*, Ω_+^*) refers to the kinematic variables of the positron in the pair rest frame and (p_r, Ω_r) to the kinematic variables of the target recoil in the CMS. We obtain:

$$d\sigma = H(X_u + P X_p) d\mu d\Omega_+^* d\Omega_r, \quad (2)$$

with:

$$H = \frac{-\alpha Z^2 r_0^2 |p_+^*| |p_r| m^2 M}{(2\pi)^2 E^3 \sqrt{s} |\vec{q}|^4}, \quad (3)$$

$$X_u = \left[\left(\frac{p_+ \sin \theta_+}{E_+ - p_+ \cos \theta_+} \right)^2 (4E_-^2 - q^2) + \left(\frac{p_- \sin \theta_-}{E_- - p_- \cos \theta_-} \right)^2 (4E_+^2 - q^2) + \frac{2p_+ p_- \sin \theta_+ \sin \theta_- \cos(\varphi_+ - \varphi_-)}{(E_- - p_- \cos \theta_-)(E_+ - p_+ \cos \theta_+)} (4E_+ E_- + q^2 - 2E^2) - 2E^2 \frac{(p_+ \sin \theta_+)^2 + (p_- \sin \theta_-)^2}{(E_+ - p_+ \cos \theta_+)(E_- - p_- \cos \theta_-)} \right], \quad (4)$$

$$X_p = \cos 2\varphi_- (4E_+^2 - q^2) \left(\frac{p_- \sin \theta_-}{E_- - p_- \cos \theta_-} \right)^2 + \cos 2\varphi_+ (4E_-^2 - q^2) \left(\frac{p_+ \sin \theta_+}{E_+ - p_+ \cos \theta_+} \right)^2 + 2 \cos(\varphi_+ + \varphi_-) (4E_+ E_- + q^2) \frac{p_- \sin \theta_- p_+ \sin \theta_+}{(E_- - p_- \cos \theta_-)(E_+ - p_+ \cos \theta_+)}. \quad (5)$$

A number of technical verifications were undertaken to check that the whole process was implemented correctly, including a comparison of the result of a calculation of the pair invariant mass based on the Bethe-Heitler variables to the value of μ .

4. The VEGAS-based generator

VEGAS is a multipurpose algorithm for multidimensional integration that was developed for particle-physics applications. It is adaptative in that it automatically concentrates evaluations of the integrand in those regions where it is largest in magnitude [21, 32]. The integral is performed on an n D grid that is the simple product of n 1D grids (here $n = 5$). Initially, the segmentation is uniform on each 1D axis. It is then iteratively modified so as to minimize the variance of the estimation of the integral.

We have used the VEGAS method in its BASES/SPRING implementation [20] to build the first generator [18]. After the grid optimisation has been performed by BASES, the pdf, i.e., the normalised differential cross section, is known on all nodes of the n D grid. The SPRING package then generates the exact pdf from the tabulated one by the acceptance-rejection method (see, example, Sect. 40.3 of [31]).

If the pdf has singularities that involve several of the variables on which the generation is performed in a correlated way, the grid optimisation does not converge to an appropriate solution and the VEGAS method is inefficient [20]. The choice of variables documented in the previous section had been made with that limitation in mind. Some of the five variables that were actually used in [18] were functions of the variables listed in Table 2, so as to minimize any 1D pdf divergence for that variable. This was done for practical purpose only (plotting etc.) since the VEGAS method deals with divergences effectively, within the correlation limitation already mentioned. This change of variables is, therefore, not detailed here.

A different set of variables is used for the new generator for which the resampling facility of the VEGAS method is not available anymore, as presented in the next section.

Table 3: Relationship between the generator variables, $x_i, i = 1 \dots 5$, and the kinematic variables, and their range.

i		Jacobian	x_i range
1	$\cos \theta = \frac{y-1}{1+y}, y = \exp(x_1)$	$\frac{y}{(1+y)^2}$	$[x_{1l}, x_{1u}]$
2	$\mu = \mu_{\min} (\mu_r)^{x_2^2}$	$2 x_2 \log(\mu_r) \mu$	$[0, 1]$
3	$\cos \theta_\ell = x_3$	$ \sin \theta_\ell $	$[0, \pi]$
4	$\phi_\ell = x_4$	1	$[-\pi, \pi]$
5	$\phi = x_5$	1	$[-\pi, \pi]$

5. The new event generator

From the study of the 1D distributions of the five variables provided by the VEGAS-based generator, we obtained a set of variables $x_i, i = 1 \dots 5$ so that each x_i takes values on a (finite length) segment and its pdf does not have any singularity.

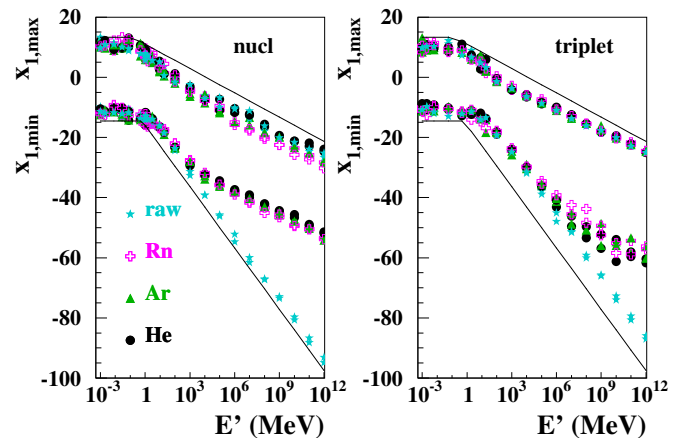


Figure 1: Variation with E' of the maximum and of the minimum values for variable x_1 . Left: nuclear conversion; Right: triplet conversion. “raw” isolated charged target (star), and the following atoms: helium (bullet), argon (upper triangle), radon (plusses). The continuous lines denote the bounds that are used by the generator. $P = 1$ and $P = 0$ samples are plotted for each photon-energy value.

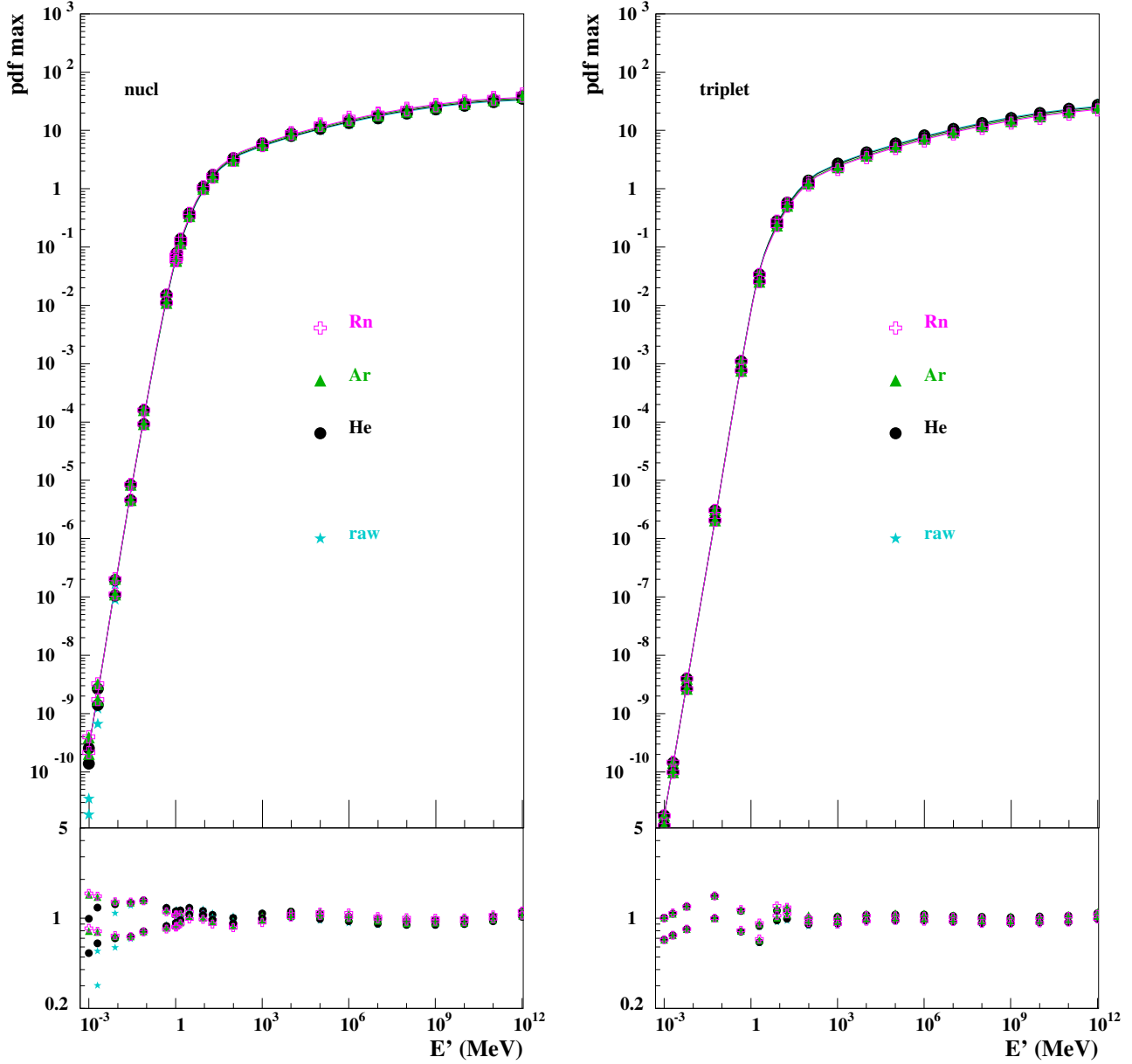


Figure 2: Top: Variation of the maximum value of the pdf (arbitrary units) with E' . Left: nuclear conversion; Right: triplet conversion. “raw” isolated charged target (star), and the following atoms: helium (bullet), argon (upper triangle), radon (plusses). The continuous lines denote the parametrisation of eq. (9). Bottom: residues of the fit of eq. (9). $P = 1$ and $P = 0$ samples are plotted for each photon-energy value.

The relation between the generator variables $x_i, i = 1 \dots 5$ and the kinematic variables is given in Table 3. $\mu_r = \mu_{\max}/\mu_{\min}$, with $\mu_{\min} = 2m$ and $\mu_{\max} = \sqrt{s} - M$. In this document log refers to the natural logarithm.

For better readability, energy-variation plots are presented as a function of

$$E' = E - E_{\text{threshold}}, \quad (6)$$

where the energy threshold is

- $E_{\text{threshold}} = 2mc^2$ for nuclear conversion and
- $E_{\text{threshold}} = 4mc^2$ for triplet conversion.

E' is the available kinetic energy of the leptons for nuclear conversion, but not for triplet conversion.

The x_1 bounds, x_{1l}, x_{1u} , are given in Fig. 1 as a function of E' . For each energy, for each target, for each process (nuclear, triplet), for each side (upper bound, lower bound), the two points correspond to fully polarised ($P = 1$) and to non-polarised ($P = 0$) simulated data. Each value is computed from a sample of 10^5 simulated events.

We take x to be the set of variables for a conversion event, $x = (x_i, i = 1 \dots 5)$, and X the physically accessible part of the 5D space for x . The variables, x , are taken at random with a uniform pdf $p_0(x) = p_0$. The exact pdf, $p(x)$, is then “carved” into that 5D-flat sample using the acceptance-rejection method: if a constant C can be found, so that for all points x ,

$$Cp_0(x) > p(x), \quad (7)$$

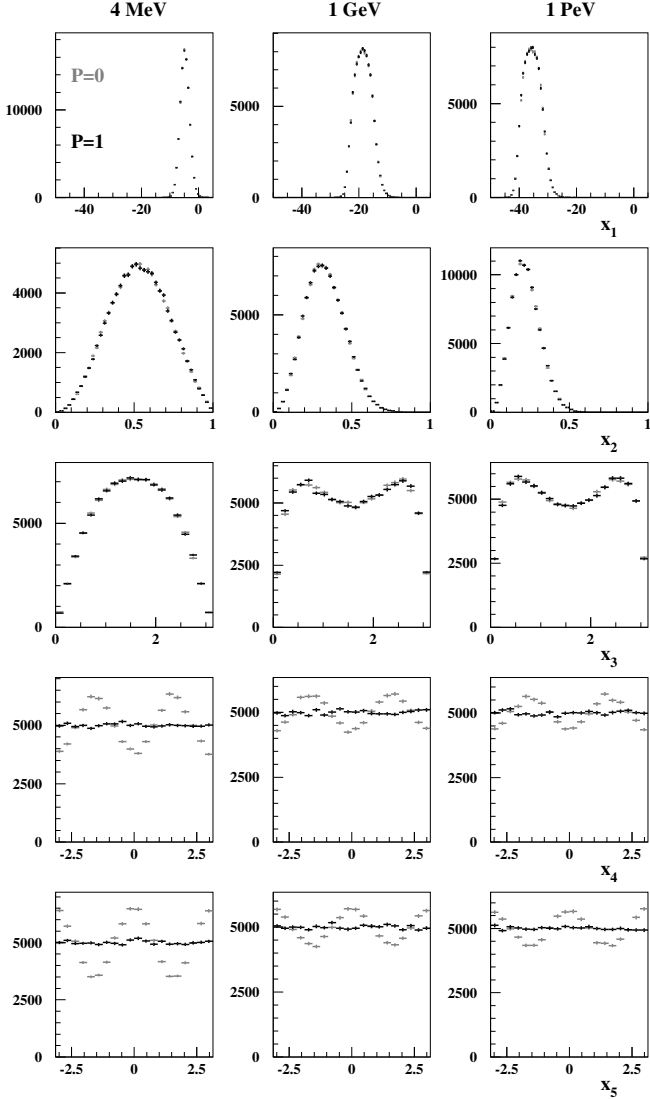


Figure 3: The distributions of the five generation variables for the nuclear conversion of γ -rays of energies 4 MeV, 1 GeV and 1 PeV on argon. $P = 1$ (grey) and $P = 0$ (black) samples are plotted for each photon-energy value.

then taking a random variable u , flat in $[0, 1]$, and accepting events for which

$$uCp_0(x) < p(x), \quad (8)$$

provides an x sample with pdf $p(x)$ (section 40.3 of [31]).

For $p_0 = 1$, C is the maximum value of $p(x)$ that we have studied with the VEGAS-based generator. It can be represented by the following function

$$\frac{\tau_1 E'^{\tau_3 + \tau_5 \log E'}}{\tau_2 E'^{\tau_6} + E'^{\tau_4}} \left(1 + \tau_8 Z^{\tau_9} \frac{Q}{1+Q} \right) \quad \text{with} \quad Q = \frac{E'}{\tau_{10}}, \quad (9)$$

where the sets of constants τ_i are different for nuclear and for triplet conversions. These expressions of the values of $C(E', Z)$ for nuclear and triplet conversions are compared to the values obtained from simulated samples in Fig. 2. In practice, for safety, C is enlarged by a factor of 1.5 with respect to what can be seen on Fig. 2. In these expressions, Z is the atomic number of the atom on which the conversion took place. The raw

data, that is, the conversion on an isolated electron or nucleus, are found to be well represented by an effective $Z = 0.5$. The distributions of the five variables do not show any remaining divergence (Fig. 3).

5.1. Total cross section

We integrate the differential cross section used by the generator and obtain the total cross section (Fig. 4).

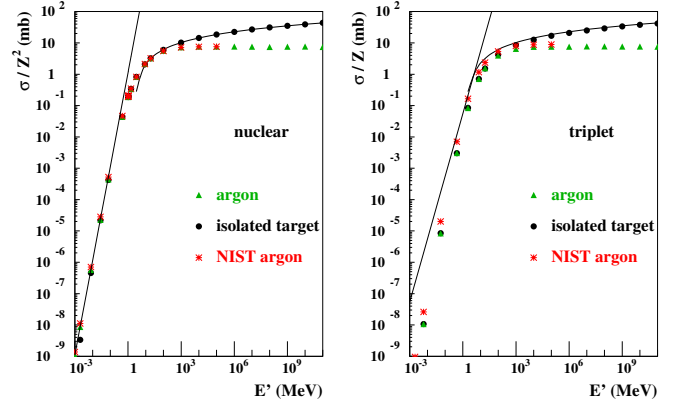


Figure 4: Total cross section normalised to $Z = 1$, as a function of E' . Left: nuclear conversion. Right: triplet conversion. Thick line: high-energy approximation. Thin line: low-energy approximation. Integration of the differential cross section used in the generator for conversion on isolated charged particles (bullets) or argon atoms (upper triangles). Values tabulated by NIST (crosses).

The thick line shows the high-energy approximation [22]

$$\sigma_{\text{tot}} = \frac{28}{9} \log \left(\frac{2E}{mc^2} \right) - \frac{218}{27}. \quad (10)$$

The thin line shows low-energy approximation. For nuclear conversion [33]

$$\sigma_{\text{tot}} = \alpha r_0^2 Z^2 \frac{\pi}{12} \left(\frac{E}{mc^2} - 2 \right)^3 \quad (11)$$

For triplet conversion we use the expression obtained using the Borsellino diagrams [34], something that is appropriate for this comparison to the Bethe-Heitler cross section based on the same assumption:

$$\sigma_{\text{tot}} = \alpha r_0^2 \frac{\pi \sqrt{3}}{2^3 3^3} \left(\frac{E}{mc^2} - 4 \right)^2. \quad (12)$$

The misprint in [34] mentioned in [35] has been corrected.

The total cross section for isolated charged particles (bullets) can be compared to the approximations (thin and thick lines). The total cross section for conversion on a charged target inside an argon atom (upper triangle) can be compared to the computations of the National Institute of Standards and Technology (NIST) Physical Reference Data and based on Ref. [36].

- At energies larger than ≈ 100 MeV, the raw cross section is found to be compatible with the high-energy approximation for both triplet and nuclear conversions.

- Cross sections on atoms are found to be compatible with that tabulated by NIST except for very-low-energy triplet conversion for which a factor of ≈ 2.44 is missing which is not surprising as the lack of the exchange diagrams in the Bethe-Heitler differential cross section is sensitive there (See the discussion in section 2 of Ref. [37]).
- The low-energy nuclear cross section is found to be compatible with the low energy approximation, but the low-energy triplet cross section is not, both for the generator and for NIST data: these data seem to support an $(E/mc^2 - 4)^3$ dependence rather than the $(E/mc^2 - 4)^2$ dependence predicted by the Borsellino [34] and by the Votruba [35] expressions, something that is not understood.

5.2. Distributions of kinematic variables

We can now examine the distributions of variables that are not easily accessible by the physics models that do not sample the full 5D differential cross section. We extend the verifications that were performed in the past with the VEGAS-based generator [18, 11, 38] to the larger energy range explored in this work with the new generator.

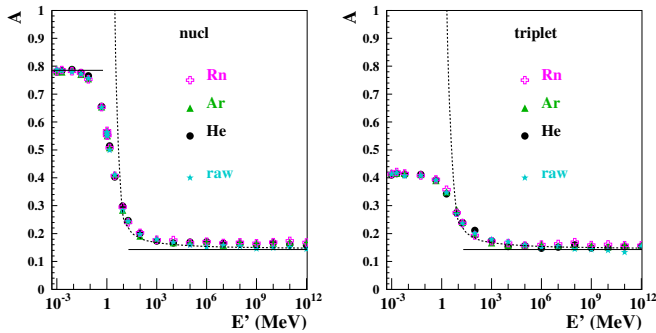


Figure 5: Polarisation asymmetry calculated on event samples simulated with the new event generator, as a function of E' . Left: nuclear conversion. Right: triplet conversion. “raw” isolated charged target (star), and the following atoms: helium (bullet), argon (upper triangle), radon (plusses). The horizontal lines denote the low- and high-energy approximations of $\pi/4$ and $1/7$, respectively. The dashed curves denote the Boldyshev-Peresunko high-energy approximation [39].

- The measurement of the polarisation angle φ_0 and of the linear polarisation fraction P of a gamma-ray beam can be performed by the analysis of the distribution of the event azimuthal angle φ

$$\frac{dN}{d\varphi} \propto (1 + A P \cos[2(\varphi - \varphi_0)]), \quad (13)$$

where A is the polarisation asymmetry of gamma conversion to pairs. Figure 5 shows the polarisation asymmetry obtained from the ($P = 1$) samples, defining the event azimuthal angle as the bisector of the electron and of the positron azimuthal angles, $\varphi \equiv (\phi_+ + \phi_-)/2$ [38], and using the moments’ method [18, 11, 38].

All (nuclear and triplet) “raw” results agree nicely with the Boldyshev-Peresunko asymptotic expression [39] at high energy²:

$$A \approx \frac{\frac{4}{9} \log(2E/mc^2) - \frac{20}{28}}{\frac{28}{9} \log(2E/mc^2) - \frac{218}{27}}. \quad (14)$$

At low energy the obtained values agree with the asymptotic value obtained in [38] for nuclear conversion but not for triplet conversion.

- As the distribution of the recoil momentum, q , has a long tail, (Fig. 3 of [13]), the contribution to the photon angular resolution $\Delta\theta$ due to the fact that the nucleus recoil cannot be measured is not Gaussian distributed: astronomers make use of the 68 %-containment resolution angle. In the transverse-recoil approximation, which is valid for $E' > 1$ MeV (Fig. 3 right of [11], $\Delta\theta$ is $\approx q/E$). Figure 6 shows the 68 %-containment value, q_{68} , of the recoil momentum, q , calculated on event samples simulated with the new event generator as a function of E' and can be compared to Figs. 3, 5 and 6 of [11].
- Figure 7 shows the distributions of the pair opening angle normalised to $1/E$ for conversions on argon. For $E > 10$ MeV, they peak at the value of 1.6 rad MeV computed by Olsen in the high-energy approximation [40].

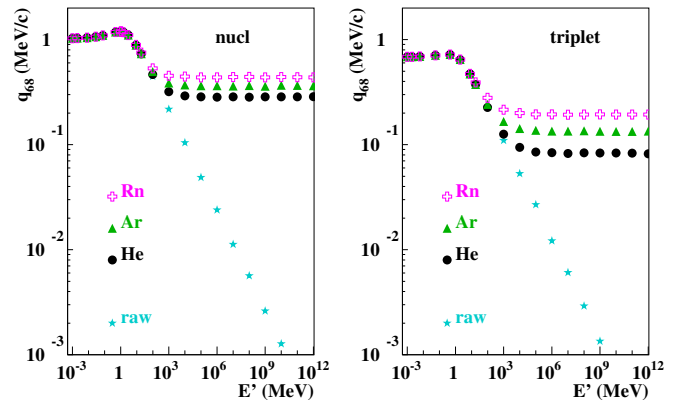


Figure 6: 68 %-containment value q_{68} of the recoil momentum q obtained from event samples simulated with the new event generator, as a function of E' . Left: nuclear conversion. Right: triplet conversion. “raw” isolated charged target (star), and the following atoms: helium (bullet), argon (upper triangle), radon (plusses).

5.3. Applicability range

The present results were obtained with REAL*16 machine precision, in the energy range from 1 keV above threshold up to 1 EeV.

²We have corrected a misprint of [38], the normalisation of the photon energy to the electron rest mass energy in the log.

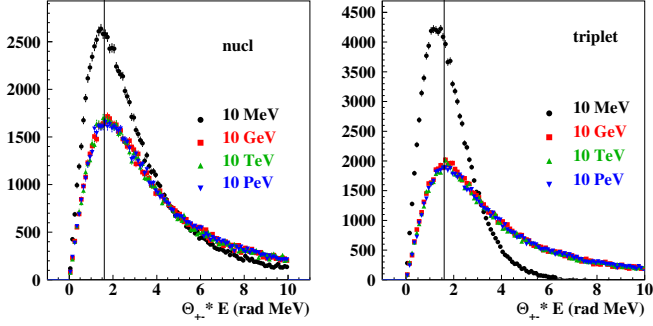


Figure 7: Distributions of the product of the pair opening angle and of the photon energy, $\theta_{+-} \times E$, for conversions on argon for 10 MeV (bullet), 10 GeV (square), 10 TeV (upper triangle) and 10 PeV (down triangle). Left: nuclear conversion. Right: triplet conversion. The vertical value shows the most probable value of 1.6 rad MeV computed by Olsen in the high-energy approximation [40].

- For conversions on nuclei or on electrons bound in atoms, the generator was found to provide nominal results, both with REAL*8 and REAL*16 machine precisions.
- For conversions on isolated charged particles and for REAL*8 machine precision, the generator is found to compute the pdf wrongly below $q \approx 10^{-8}$ MeV/c, which can be reached for γ -ray conversions above $E \approx 40$ TeV. Conversions on atoms are immune to this limitation because screening prevents conversions with such low values of q .

Note that the CPU time increases with precision, from 0.22 ms/event (REAL*8) to 6.6 ms/event (REAL*16) for 100 MeV γ -ray nuclear conversions on argon, on a DELL Precision M4600 machine.

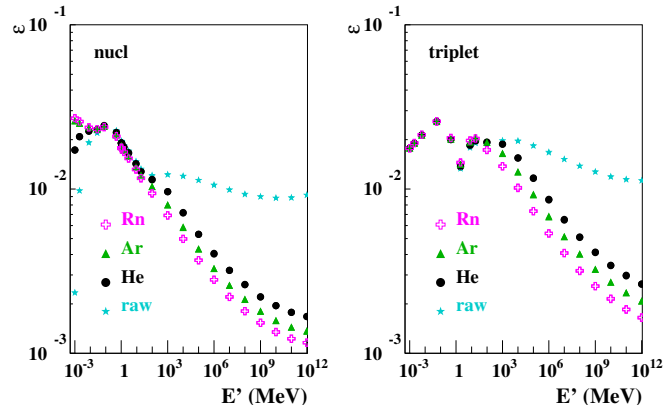


Figure 8: Efficiency of the new event generator, as a function of E' . Left: nuclear conversion. Right: triplet conversion. “raw” isolated charged target (star), and the following atoms: helium (bullet), argon (upper triangle), radon (plusses).

5.4. Generator efficiency

The efficiency of the generator, ϵ , defined as the inverse of the average number of computations of the pdf needed to obtain one generated event, is low, between one-per-mille and several

percent, (Fig. 8), which is a sign of large correlations among the variables. Therefore, it might be wise to restrict the use of this physical model to the primary interaction of a photon in a detector and not to the generation of a full EM shower.

We tried to find changes of variables on x_1 or x_2 to make the 1D pdfs flatter in the hope of improving the overall generator efficiency and we did not succeed. So we took x_1 at random after a 1D pdf, which is equivalent to a change of variable.

We first tried to take x_1 at random with pdf $p_1(x_1) \equiv \int p(x) dx_2 dx_3 dx_4 dx_5$, where the integral is performed numerically. We use the acceptance-rejection method described in Sect. 3 on pdf $p(x)/p_1(x_1)$ instead of using it on pdf $p(x)$, which is equivalent to a Jacobian factor correction. We were not able to fine-tune this method because, due to the already-mentioned correlations, some events have a large value of $p(x)$ even though they have a small value of $p_1(x_1)$, so the value of $p(x)/p_1(x_1)$ can be extremely high, making the determination of C inefficient.

Taking instead x_1 at random with pdf $p'_1(x_1) \equiv \max_{x_2, \dots, x_5} p(x)$, a function that we parametrised with parameters described as functions of (E, Z) separately for nuclear and triplet conversions resulted in an efficiency gain by a factor two to three in the (E, Z) range considered in this work. This shows that indeed the low efficiency is intimately related to the correlations amongst the variables.

6. Conclusion

We have developed a 5D, exact, polarised, Bethe-Heitler event generator of γ -ray conversions to e^+e^- that is able to simulate successive events with different photon energies and different atomic targets without any CPU overhead. The strong correlation between kinematic variables in the divergence of the five-dimensional differential cross section was mitigated by performing each step of the conversion in the appropriate Lorentz frame. We have performed a number of verifications by comparison with properties established in the past from analytical calculations, on the photon energy range from 1 keV above threshold up to 1 EeV. The calculation is currently implemented in fortran; it can be implemented in other programming languages.

7. Acknowledgments

It is a pleasure to acknowledge the support of the French National Research Agency (ANR-13-BS05-0002).

References

- [1] S. Agostinelli *et al.* [GEANT4 Collaboration], “GEANT4: A Simulation toolkit,” Nucl. Instrum. Meth. A **506** (2003) 250.
- [2] J. Allison *et al.*, “Recent Developments in Geant4,” Nucl. Instrum. Meth. A **835** (2016) 186.
- [3] H. Hirayama *et al.*, “The EGS5 code system,” SLAC-R-730, KEK-2005-8, KEK-REPORT-2005-8, version: January 13, 2016.
- [4] A. Bielajew, “Improved angular sampling for pair production in the EGS4 code system”, PIRS-0287, 1991, revised version 1994.
- [5] I. Kawrakow, “Accurate condensed history Monte Carlo simulation of electron transport. I. EGSnrc, the new EGS4 version”, Medical Physics **27** (2000) 485.
- [6] F. Salvat, “The penelope code system. Specific features and recent improvements,” Annals Nucl. Energy **82** (2015) 98.
- [7] W. L. Thompson, “MCNP, A General Monte Carlo Code For Neutron And Photon Transport: A Summary,” LA-8176-MS, 1979.
- [8] G. Battistoni *et al.*, “Overview of the FLUKA code”, Annals of Nuclear Energy **82** (2015) 10.
- [9] W. R. Nelson and C. Field, “Comparison of EGS5 Simulations with Experiment,” Nucl. Instrum. Meth. A **572** (2007) 1083.
- [10] J. Apostolakis *et al.*, “Progress in Geant4 Electromagnetic Physics Modelling and Validation,” J. Phys. Conf. Ser. **664** (2015) 072021.
- [11] P. Gros *et al.* [HARPO Collaboration], “ γ -ray telescopes using conversions to e^+e^- pairs: event generators, angular resolution and polarimetry,” Astropart. Phys. **88** (2017) 60 [arXiv:1612.06239 [astro-ph.IM]].
- [12] M. Ackermann *et al.* [Fermi-LAT Collaboration], “The Fermi Large Area Telescope On Orbit: Event Classification, Instrument Response Functions, and Calibration,” Astrophys. J. Suppl. **203** (2012) 4, [arXiv:1206.1896 [astro-ph.IM]].
- [13] D. Bernard, “TPC in gamma-ray astronomy above pair-creation threshold,” Nucl. Instrum. Meth. A **701**, 225 (2013), [Erratum-ibid. A **713**, 76 (2013)], [arXiv:1211.1534 [astro-ph.IM]].
- [14] A. De Angelis *et al.* [e-ASTROGAM Collaboration], “The e-ASTROGAM mission,” Exper. Astron. **44** (2017) 25, [arXiv:1611.02232 [astro-ph.HE]].
- [15] J. Perkins, “All-Sky Medium Energy Gamma-ray Observatory (AMEGO) - A discovery mission for the MeV gamma-ray band”, 7th International Fermi Symposium, October 2017, Garmisch-Partenkirchen
- [16] S. Takahashi *et al.*, “GRAINE project: The first balloon-borne, emulsion gamma-ray telescope experiment,” PTEP **2015** (2015) 043H01.
- [17] K. Ozaki *et al.*, “Demonstration of polarization sensitivity of emulsion-based pair conversion telescope for cosmic gamma-ray polarimetry,” Nucl. Instrum. Meth. A **833** (2016) 165.
- [18] D. Bernard, “Polarimetry of cosmic gamma-ray sources above e^+e^- pair creation threshold,” Nucl. Instrum. Meth. A **729** (2013) 765, [arXiv:1307.3892 [astro-ph.IM]].
- [19] P. Gros *et al.*, “Performance measurement of HARPO: A time projection chamber as a gamma-ray telescope and polarimeter,” Astropart. Phys. **97** (2018) 10 [arXiv:1706.06483 [astro-ph.IM]].
- [20] S. Kawabata, “A New version of the multidimensional integration and event generation package BASES/SPRING,” Comput. Phys. Commun. **88** (1995) 309.
- [21] G. P. Lepage, “A New Algorithm for Adaptive Multidimensional Integration,” J. Comput. Phys. **27** (1978) 192.
- [22] H. Bethe and W. Heitler, “On the Stopping of Fast Particles and on the Creation of Positive Electrons”, Proceedings of the Royal Society of London A, **146** (1934) 83.
- [23] T. H. Berlin and L. Madansky, “On the Detection of gamma-Ray Polarization by Pair Production”, Phys. Rev. **78** (1950) 623.
- [24] M. M. May, “On the Polarization of High Energy Bremsstrahlung and of High Energy Pairs”, Phys. Rev. **84** (1951) 265.
- [25] Jauch and Rohrlich, *The theory of photons and electrons*, (Springer Verlag, 1976).
- [26] K. J. Mork, “Pair Production by Photons on Electrons”, Phys. Rev. **160** (1967) 1065.
- [27] N.F. Mott, H.S.W. Massey, “The Theory of Atomic Collisions”, University Press, Oxford, 1934.
- [28] J.A. Wheeler and W.E. Lamb, “Influence of atomic electrons on radiation and pair production”, Phys. Rev. **55** (1939) 858 (errata in **101** (1956) 1836).
- [29] L. D. Landau and I. Pomeranchuk, “Limits of applicability of the theory of bremsstrahlung electrons and pair production at high-energies,” Dokl. Akad. Nauk Ser. Fiz. **92** (1953) 535.
- [30] A. B. Migdal, “Bremsstrahlung and pair production in condensed media at high-energies,” Phys. Rev. **103** (1956) 1811.
- [31] C. Patrignani *et al.* [Particle Data Group], “Review of Particle Physics,” Chin. Phys. C **40** (2016) 100001.
- [32] G. P. Lepage, “Vegas: An Adaptive Multidimensional Integration Program,” CLNS-80/447, 1980.
- [33] Racah G., “Sulla Nascita Degli Elettroni Positivi”, Nuovo Cim. **11** (1934) 477.
- [34] A. Borsellino, “Sulle coppie di elettroni create da raggi gamma in presenza di elettroni”, Nuovo Cim. **4** (1947) 112.
- [35] V. Votruba, “Pair production by gamma-rays in the field of an electron”, Phys. Rev. (Lett. to Ed.) **73** (1948) 1468.
- [36] J. H. Hubbell, H. A. Gimm, and I. Overbo, “Pair, Triplet, and Total Atomic Cross Sections (and Mass Attenuation Coefficients) for 1 MeV -100 GeV Photons in Elements Z=1 to 100”, J. Phys. Chem. Ref. Data **9** (1980) 1023.
- [37] J. Joseph and F. Rohrlich, “Pair Production and Bremsstrahlung in the Field of Free and Bound Electrons”, Rev. Mod. Phys. **30** (1958) 354.
- [38] P. Gros *et al.* [HARPO Collaboration], “ γ -ray polarimetry with conversions to e^+e^- pairs: polarization asymmetry and the way to measure it,” Astropart. Phys. **88** (2017) 30 [arXiv:1611.05179 [astro-ph.IM]].
- [39] V. F. Boldyshev and Y. .P. Peresunko, “Electron-positron pair photoproduction on electrons and analysis of photon beam polarization,” Yad. Fiz. **14** (1971) 1027.
- [40] H. Olsen, “Opening Angles of Electron-Positron Pairs,” Phys. Rev. **131** (1963) 406.